

Micro-injection Moulding of Lab-on-a-chip(LOC)

HwaJin Oh¹, JaeHong Park², YoungSeok Song³, and JaeRyoun Youn¹

¹ Seoul National University, Seoul, Korea.

² National NanoFab Center, Deajeon, Korea.

³ Dankook University, Gyeong-gi Do, Korea

ABSTRACT

we demonstrate a sustainable fabrication platform to micromould a lab-on-a-chip device with multiscaled microstructures. To the best of our knowledge, this is the first report not only preparing the whole microfluidic device instead of a simple single microstructure using microinjection moulding but also introducing a numerical tool that helps illustrate how micro- and macro-sized cavities are filled through the multiscale simulation approach in a straightforward manner. Furthermore, we proposed a new dimensionless characteristic number, the microfilling number (μ_f) to better understand the underlying physics of microinjection moulding and relevant key factors of determining the replication quality of micromoulded parts.

INTRODUCTION

A small scale platform where manifold physical and chemical operations are allowed, the so-called lab-on-a-chip has shown a capability of analyzing biological and chemical samples with a microfluidic system.¹⁻³ Such a platform offers new fascinating methods to a wide variety of areas including biology,^{4, 5} chemistry,⁶ medical,⁷ pharmacology,⁸ tissue engineering,⁹ and mechanics,¹⁰⁻¹² where a small amount of liquid can minimize the time, cost, space and even labor necessary for handling the analyzing samples with high

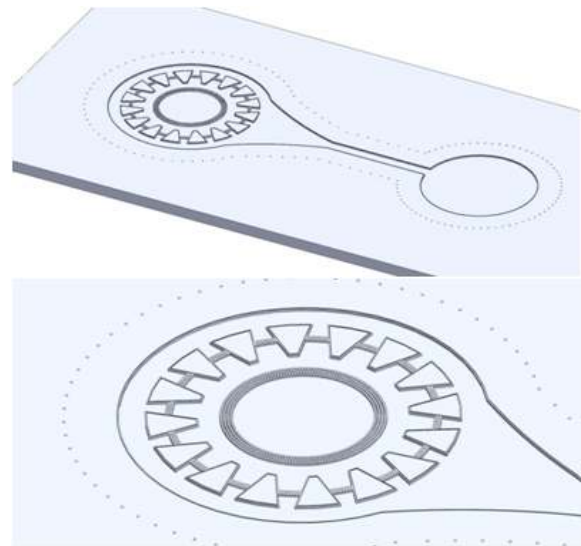
efficiency and speed. In particular, the precise control of fluid on a microscale enables one to manipulate even molecular level analytes and to take advantage of the unique feature of microflow, which can also meet the demand for portable point-of-care (POC) device for public health without the help of an expert operator in centralized hospitals.¹³⁻¹⁵ Indeed, while the microfluidic system has some drawbacks such as unstable flow possibility, the aforementioned advantages of lab-on-a-chip devices seem too compelling to let pass.¹⁶⁻¹⁹ However, now that production of that devices still remain challenging due to the lack of exploitation for commercialization, the devices have not yet become widely used in our ordinary lives.²⁰⁻²³ On the other hand, injection moulding is a process well known as one of the most efficient processes for the large-scale production of polymeric microparts in terms of its good replication capability and excellent processability. Thus far, a tremendous amount of effort has been made to manufacture polymeric products with microstructures such as light-guide plate,²⁴ microlens,²⁵ optical storage,²⁶ and sensors²⁷ in more robust manner. In order to materialize these microfeatured components, which also act as key elements in many cutting edge industries, injection moulding is recently being adopted.^{28, 29} The so-called microinjection moulding involves more complicated natures compared with either

conventional injection moulding or other moulding processes such as hot embossing and thermoforming.³⁰ For instance, microcavities tend to be unfilled during the filling process of injection moulding due to high surface tension of a molten polymer and thicker skin layer than the size of the microcavities, thus resulting in unsatisfactory replication quality of products.^{24, 29} In the realm of injection moulding simulation, it is very difficult to numerically model the injection moulding processes of an entire part but not one single unit cell owing to low computational power (e.g., parallel computing).^{31, 32}

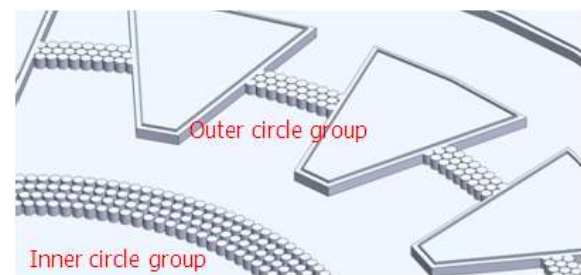
EXPERIMENTAL

Insert Design

As design for pillar-shaped micro structure moulding experiment using plastic injection moulding, circle patterns are radially arrayed in 360° to form radial pillar group (Fig. 1). Diameter of each circle is divided into two groups of 100 μm and 20 μm, and it is also designed for the target moulding height to be 20 μm. The whole diameter of the circle group with 100 μm of diameter is about 10 mm, and the whole diameter of the circle group with 20 μm of diameter is 6 mm approximately. The inner array group of circles with diameter of 20 μm has distance of 20 μm to 10 μm in between and is designed to have 4 layer toward center of radial. Also, the outer array group of circles with diameter of 100 μm has distance of 20 μm to 10 μm in between and is designed to have 4 layer toward center of radial. (Designed pattern above has specific microstructures to test particular function of plastic type Lab on a Chip for biochip application. The concrete meaning of the design is not handled in this research)



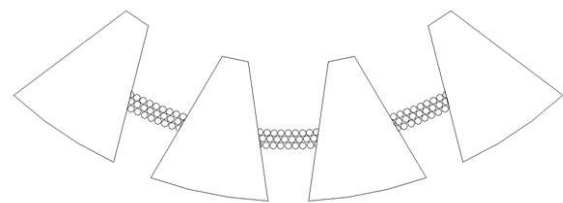
(a)



(b)



(c)



(d)

Figure 1. Schematic illustration of micropatterned lab-on-a-chip (LOC). (a) Entire image of the designed LOC device (top) and magnified image of its inlet (bottom). (b) Layout of the microstructures on the LOC chip. (c) Magnified image of two micropillar groups, i.e., the outer circle group and the inner circle group. (d) Magnified top view of the outer circle group pillars and the flow guiding trapezoidal pillars.

Flow chart of process to fabricate polymeric COC (Cyclic Olefin Copolymer) with target pillar-shaped micro structure on the basis of examined design as shown in figure 2(a).

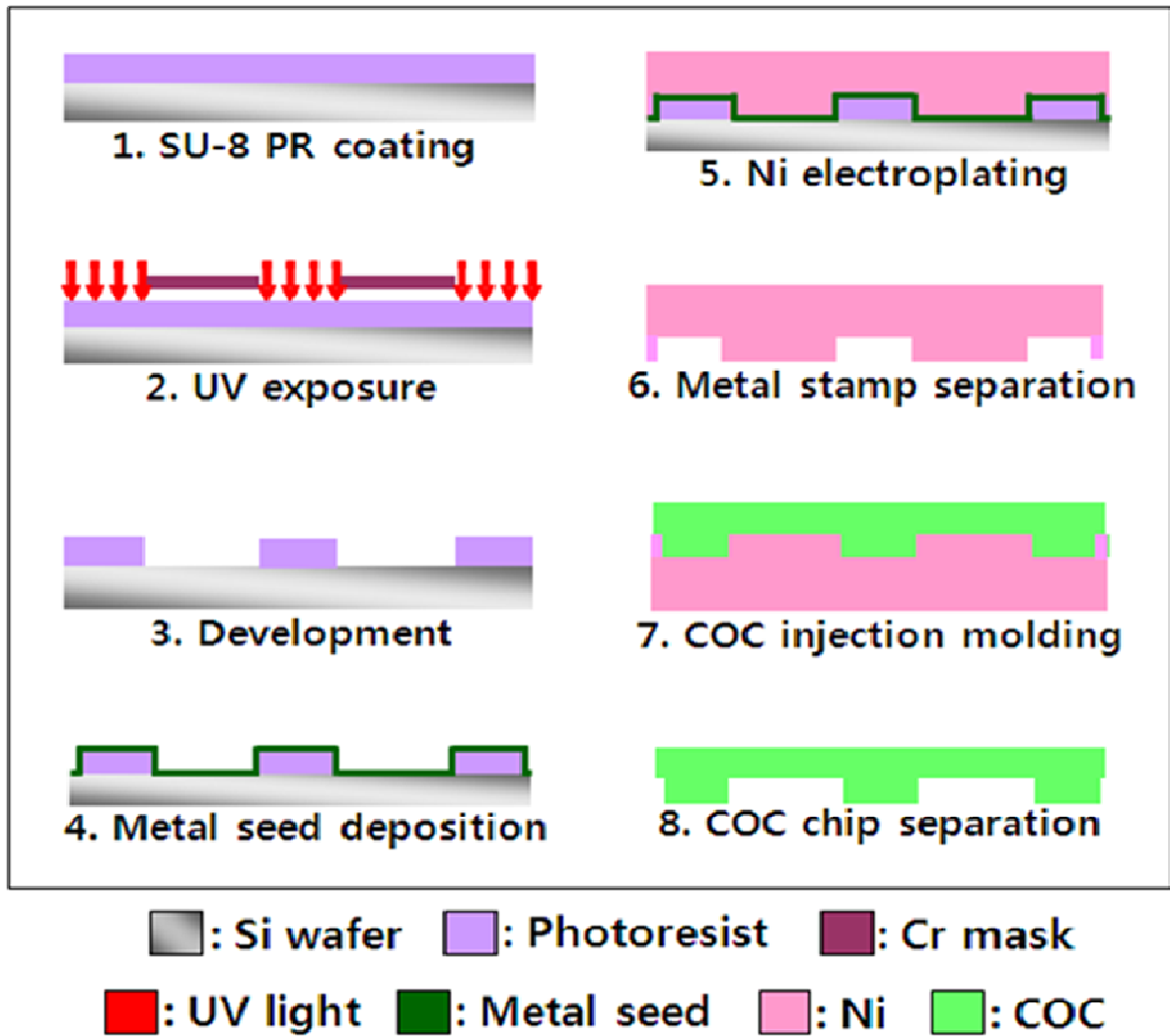
To materialize designed geometry (pillar shaped micro structure), it is necessary to fabricate metal stamp which has the complementary structure. First of all, to fabricate Cr mask for photolithograph process, photo mask with width of 7 inch and height of 7 inch was fabricated using mask generator (DWL 200, Heidelberg Instruments, Germany).

Using <100> Si wafer with size of 6 inch as board, Ti and Cr were vacuum-evaporated in thickness of 200Å and 2000Å respectively with metal seed layer for plating. The reason why Titanium and Chrome are vacuum-evaporated is that Titanium enhances adhesive strength between Chrome and Silicon wafer and Chrome perform a role of conductive seed layer necessary for Ni electroplating process will be carried out later.

After coating Si wafer on which seed layer is vacuum-evaporated with PR (Photoresist) in desired thickness, patterning was carried out with PR through photolithography. First of all, PR (THB 151N, JSR corp) with thickness of 20 μm was materialized using spin coating method. PR's thickness is channel's depth when COC chip is fabricated. In this research, negative photoresist (THB 151N) was chosen to remove photoresist easily after Ni electroplating carried out after photolithography. In this experiment, condition of rotary application is divided into 2 steps, and the 1st step was carried out in 300 rpm and the 2nd step was carried out in 500 rpm. Because viscosity of photoresist is high, it is divided into 2 steps for application with constant thickness on wafer. Also for application with constant thickness, it is recommended to leave it on flat place for 2 hours after rotary application. After time for

stabilizing, soft bake process was carried out at 120 °C for 40 min using convection oven. After soft bake process, mask aligner (EVG640, Austria) was used to transfer pattern on fabricated mask onto wafer on which photoresist was applied. Applied total energy of UV light is 2,200 - 2,400 mJ/cm² using mask aligner. Micro structure composed of PR was materialized using developer (DVL2000, JSR corp.) after exposure.

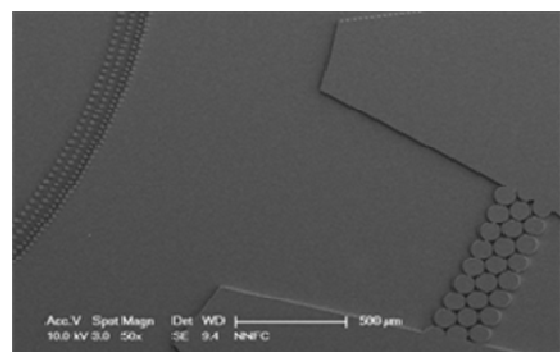
Chrome with thickness of 1000Å, as 2nd metal seed layer, was vacuum-evaporated on the fabricated wafer using E-beam evaporator. The reason why the 2nd metal seed layer is vacuum-evaporated is to carry out Ni electroplating on whole photoresist pattern mould. To remove potential bubble between micro structures materialized on wafer, vacuum pump was used to remove bubble before Ni electroplating. To minimize stress of Nickel plated on Ni electroplating, plating was carried out in 5 steps increasing current intensity successively from low current intensity. Plating was carried out with current of 100 mA - 500 mA for 60 min in the 1st step, current of 600 mA - 1000 mA for 60 min in the 2nd step, current of 1100 mA - 2000 mA for 60 min in the 3rd step, current of 3500 mA - 4000 mA for 60 min in the 4th step, and current of 7000 mA for 60 min in the 5th step. With the 5 steps of plating, Ni was vacuum-evaporated with thickness of 100 μm - 150 μm along the micro structure materialized on wafer. After that, about 1000 μm thickness of Ni plate was gained using relatively high current (approximately 1A level). After Ni electroplating, Ni plate was cut into proper size with wire cutting method for installation on mould of injection moulding equipment. In order to identify the fabrication of micro-pillars, the surface of Ni plate was observed by an atomic force microscope (AFM) (XE-100, PSIA, Korea) as shown in figure 2(b). A z-scanner was additionally used to prevent the x-z cross



(a)



(b)



(c)

Figure 2. (a) Schematic diagram of fabrication of a metal stamp and a LOC device by photolithography and electroplating. (b) Cross-sectional image of the metal stamp micropillar. (c) SEM image of the LOC produced by microinjection moulding.

coupling problem of AFM.

Injection Moulding

Micro-hole pattern-structured Ni stamp, of which polishing is completed, was installed on mould of PMIM (Plastic Micro Injection Mould, 270C 400-100, Arburg Co.). COC (Cycloolefin Copolymer, TOPAS advanced polymers Co.) material, which has bead shape with diameter of 1mm approximately, was adopted for dehumidifier (Purpose VHM5-LC, HANSE cop) and it was dried at 70 °C for 5 hr in vacuum environment. Subsequently, temperature from PMIM's material melting cylinder to nozzle was set from 305 °C to 330 °C, which is melting point for COC material, stage by stage. After temperature of mould to target temperature, it was warmed up for 3 hr to secure enough time for thermal conduction & thermal equilibrium. Figure 2(c) is the SEM image of the microstructure of fabricated micro-structured lab on a chip by an injection moulding.

MULTI-SCALE SIMULATION

In the case of a simulation with both macro and micro scale objects, multi-scale method is necessary to progress the injection moulding of a macro moulded part with micro structures. There are two scales in our specimen, micro pillars (tens and hundreds micrometers) and macro cavity (tens centimeters). It is irrational to simulate the micro-structured moulded part all together. It requires long computational time as too many meshes were generated to describe the micro-structured pillars in a whole moulded part. As shown in (a) and (b) of figure 3, domain 1 includes a whole part of the lab-on-a-chip and domain 2 is a local part of it. Domain 1 was consisted of about 500 millions elements, 3-D tetrahedral, to solve the governing equations in the figure 3(c). The figure 3(d) and (e) show the meshes of micro pillars in the domain 2. The average element size of meshes in the domain 2 was

about 1 micrometer to satisfy conditions for solving the governing equations based on FEM successfully.

The results of velocity and temperature field from the domain 1 applied to boundary conditions of the domain 2 to calculate the multi scale problem in this study. It was assumed that the inside surfaces of the domain 2 have insulated property for no heat change. And the mould temperature at each process was applied to the surface to a mould wall, having pillars, as the boundary condition for the energy conservation. Also the boundary conditions of the velocity in domain 2 could be calculated from the momentum equation in the domain 1 respectively.

RESULTS AND DISCUSSION

The simulation was successfully performed for a lab-on-a-chip with microstructures. As shown in figure 3(f), it was simulated in the macro-scale that the COC polymer melt injected to the cavity (domain 1) with simplified micro-pillars. From the calculation of velocity and temperature field for the domain 1, boundary conditions for the domain 2 were obtained respectively. And then the micro-scale simulation was carried out to describe the fill of micro-pillars as illustrated in figure 3(g).

There are many factors influencing on shape and physical properties of an injection moulded part. Most important things are the mould temperature and packing pressure of a process from previous researches^{24, 28}. These are investigated to confirm the major factor of an injection moulded part with microstructures in this study. The effect of pressure on the microstructure, a less related influential factor, was mentioned on the supplementary information. As shown in Figure 4(a), the effect of the mould temperature was definite that increasing the temperature caused higher filling ratio of the micro-pillar of 20 μm height and larger top-surface of the micro-pillar of 100 μm . Both 20 and 100 μm pillars are fully filled at the mould temperature of 135 °C. In order to

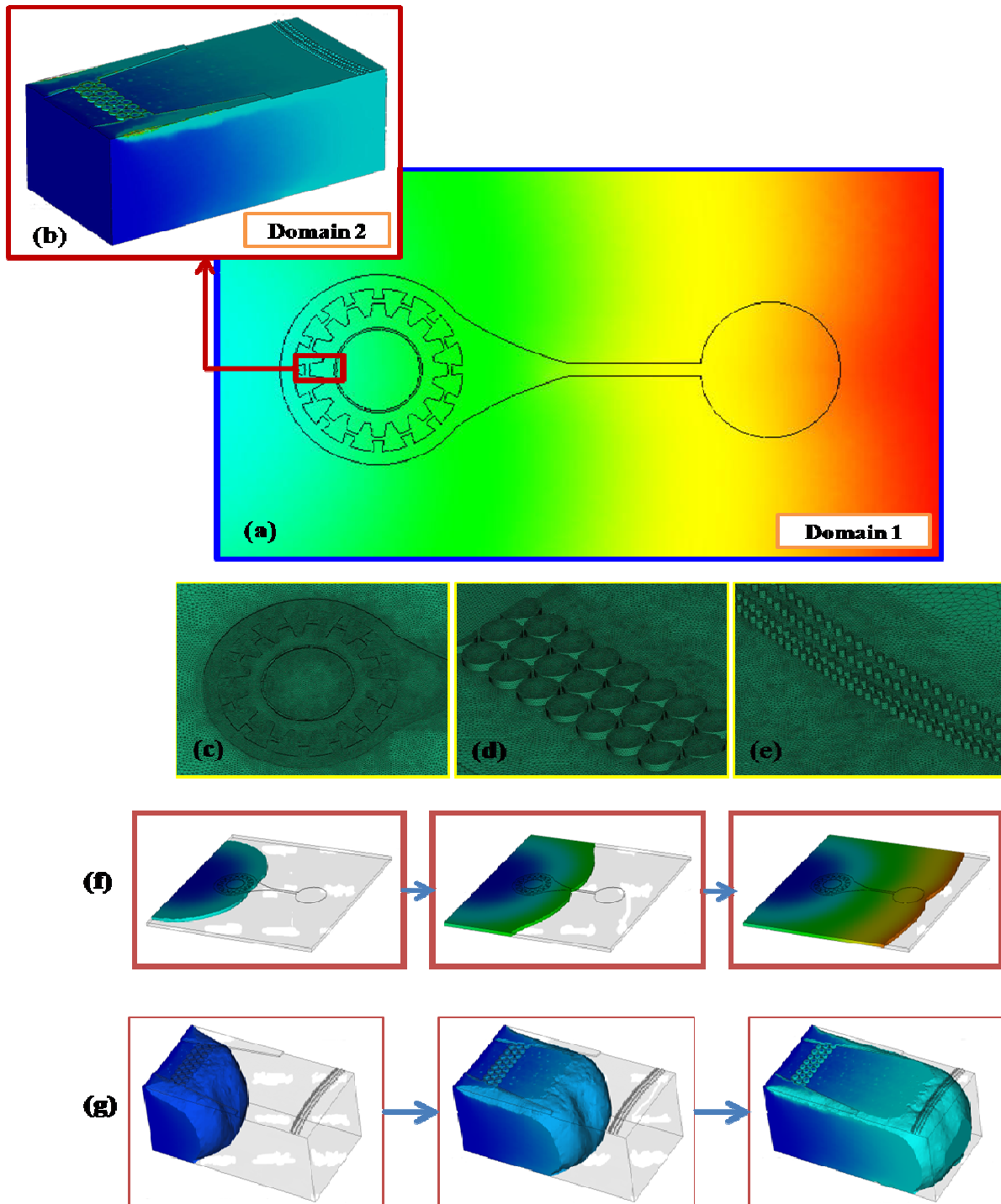
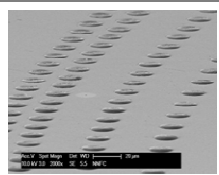
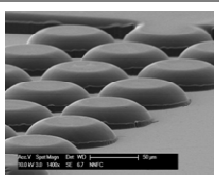
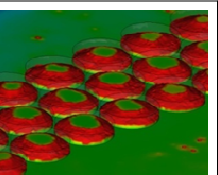
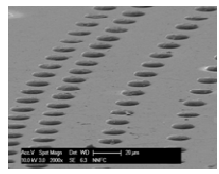
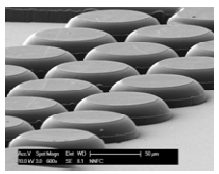
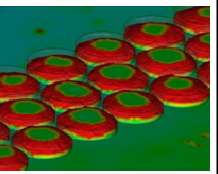
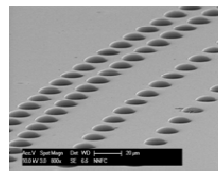
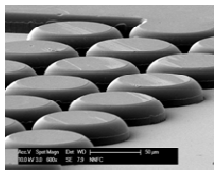
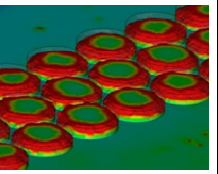
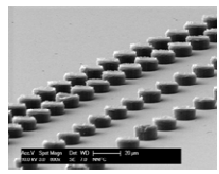
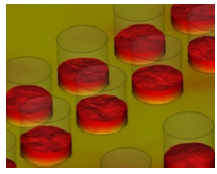
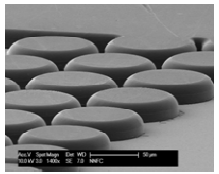
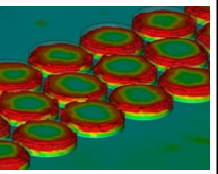
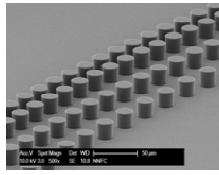
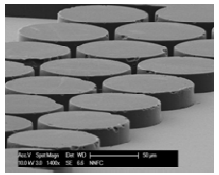
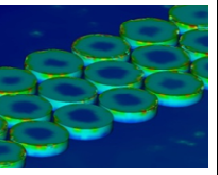
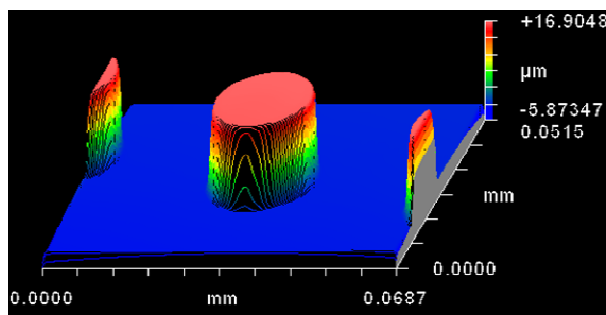


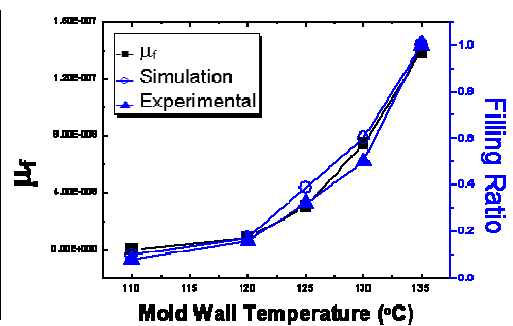
Figure. 3. Characterization of the mould filling behaviour through multiscale analysis. (a) Computation domain for the entire LOC, where the colour spectrum from blue to red indicates the fill time of the macroscopic cavity. (b) Computation domain for the microscopic cavity taken from the domain 1. (c) Image of the finite element mesh for the circular inlet microstructure composed of the outer circle group and the inner circle group pillars. (d) Image of the finite element mesh for the outer circle group pillars. (e) Image of the finite element mesh for the inner circle group pillars. (f) Snapshots of the melt front moving forwards in domain 1 over time. (g) Snapshots of the melt front moving forwards in domain 2 over time.

	Pillar with diameter of 20 μm		Pillar with diameter of 100 μm	
Mold temperature ($^{\circ}\text{C}$)	Experimental	Simulation	Experimental	Simulation
110				
120				
125				
130				
135				

(a)



(b)



(c)

Figure 4. Filling behavior for micropillars in microinjection molding. (a) Comparison between experimental and numerical results for two different types of pillars with different diameters of 20 μm and 100 μm , respectively. (b) Profilometer image of a micropillar with a 20 μm diameter. (c) Plot of the filling ratios obtained experimentally and numerically with respect to mold wall temperature and their quantitative comparison with the microfilling number.

measure the height of pillars, one of them was examined by a profilometer. For instance figure 4(b) shows the shape of a pillar made at 135 °C. The measured heights of pillars at each case are plotted with calculated values by using the FEM in figure 4(c). Furthermore the dimensionless number, μ_f , was created to explain physical phenomena that polymer resin fills micro-pillars during an injection moulding process. The micro-filling number, μ_f , was defined as:

$$\mu_f = \text{Re}_R \text{Nu}_R \tilde{T} \quad (8)$$

where Re is the Reynolds number, Nu_R is the Nusselt number, and \tilde{T} is the dimensionless glass transition temperature expressed as $(T_g - T_r)/(T_w - T_r)$. T_g is the glass temperature of the polymer and T_r , T_w are the temperature of resin and mould wall.

Dimensionless numbers has included physical interpretation for these sophisticated phenomena. The Reynolds number is influenced by the viscosity and velocity of polymer melt, which means low viscosity and high velocity induce the high value of the Reynolds number. The Reynolds number increased with the mould wall temperature because the polymer melt had low viscosity in higher mould wall temperature in this processes. And the Nusselt number included the heat transfer coefficient of metal mould, the thermal conductivity of polymer melt and the thickness of solidified layer. The Nusselt number decreased with increasing the mould wall temperature due to reducing the thickness of solidified layer. But the dimensionless glass transition temperature increased with the mould wall temperature. Consequently, the multiplication of three dimensionless numbers defined as the micro-filling number during the injection moulding. It indicated the ratio of

micro-pillar filling as shown in the figure 4(c), not a same scale. But it is noticed that the height of micro-pillars can be controlled by the mould wall temperature included in the predictor, μ_f .

CONCLUSION

We have investigated injection moulding with micro-features experimentally and numerically. And the dimensionless number was established to validate physical phenomenon which contained the heat transfer and thermodynamics. The micro-filling number connotes the effect of velocity of resin flow, the ratio of viscosity and temperature gradient, and the heat transfer by mould wall temperature. To achieve computational efficiency, the multi-scale method was introduced to solve thermal flow problems related with filling of micro pillars in numerical simulation. It was a useful mean describing the micro pillars within a macro part as a decoupled solution. Experiment, injection moulding with the insert engraved with micro patterns, was performed to argue relationship between the height of pillars and physical condition, respectively. The mould insert with micro patterns was precisely manufactured by the MEMS process, and then chips were fabricated.

Microfluidic lab-on-a-chip having different height of micropillars from an insert mould can be manufactured by controlling processing condition, especially mould wall temperature. It was demonstrated by the numerical simulation and the dimensionless number.

ACKNOWLEDGMENTS

This research was supported by Basic Science Research Program through the National Research Foundation of Korea (NRF) funded by the Ministry of Education, Science and Technology(2010-0006337) Also, this study was supported by the Korea Science and Engineering Foundation

(KOSEF) grant funded by the Korean government (MEST) (R11-2005-065) through the Intelligent Textile System Research Center (ITRC). The authors are grateful for the support.

REFERENCES

1. J. El-Ali, P. K. Sorger, K. F. Jensen(2006), *Nature*, **442**, 403.
2. A. Groisman, C. Lobo, H. Cho, J. K. Campbell, Y. S. Dufour, A. M. Stevens, A. Levchenko(2005), *Nat Methods*, **2**, 685.
3. W. Sparreboom, A. van den Berg, J. C. Eijkel(2009), *Nat Nanotechnol*, **4**, 713.
4. E. Leclerc, B. David, L. Griscom, B. Lepioufle, T. Fujii, P. Layrolle, C. Legallaisa(2006), *Biomaterials*, **27**, 586.
5. S. M. Kim, S. H. Lee, K. Y. Suh(2008), *Lab Chip*, **8**, 1015.
6. N. Szita, P. Boccazzi, Z. Zhang, P. Boyle, A. J. Sinskey, K. F. Jensen(2005), *Lab Chip*, **5**, 819.
7. X. Hu, P. H. Bessette, J. Qian, C. D. Meinhardt, P. S. Daugherty, H. T. Soh(2005), *Proc Natl Acad Sci U S A*, **102**, 15757.
8. J. L. Tan, J. Tien, D. M. Pirone, D. S. Gray, K. Bhadriraju, C. S. Chen(2003), *Proc Natl Acad Sci U S A*, **100**, 1484.
9. C. Jamora, E. Fuchs(2002), *Nat Cell Biol*, **4**, E101.
10. J. C. Martin, J. N. Marhefka, B. Kalman, D. Hudson(2010), *Adv Mater*, **23**, 426.
11. C. J. Bettinger, H. A. Becerril, D. H. Kim, B. L. Lee, S. Lee, Z. Bao(2011), *Adv Mater*, **23**, 1257.
12. Y. S. Song, D. Adler, F. Xu, E. Kayaalp, A. Nureddin, R. M. Anchan, R. L. Maas, U. Demirci(2010), *Proc Natl Acad Sci U S A*, **107**, 4596.
13. D. B. Weibel, G. M. Whitesides(2006), *Curr Opin Chem Biol*, **10**, 584.
14. F. K. Balagadde, L. You, C. L. Hansen, F. H. Arnold, S. R. Quake(2005), *Science*, **309**, 137.
15. P. Yager, T. Edwards, E. Fu, K. Helton, K. Nelson, M. R. Tam, B. H. Weigl(2006), *Nature*, **442**, 412.
16. G. M. Whitesides(2006), *Nature*, **442**, 368.
17. S. Xu, Z. Nie, M. Seo, P. Lewis, E. Kumacheva, H. A. Stone, P. Garstecki, D. B. Weibel, I. Gitlin, G. M. Whitesides(2005), *Angew Chem Int Ed Engl*, **44**, 724.
18. P. S. Dittrich, A. Manz(2006), *Nat Rev Drug Discov*, **5**, 210.
19. Y. S. Song, R. L. Lin, G. Montesano, N. G. Durmus, G. Lee, S. S. Yoo, E. Kayaalp, E. Haeggstrom, A. Khademhosseini, U. Demirci(2009), *Anal Bioanal Chem*, **395**, 185.
20. D. Psaltis, S. R. Quake, C. Yang(2006), *Nature*, **442**, 381.
21. D. Janasek, J. Franzke, A. Manz(2006), *Nature*, **442**, 374.
22. J. Fu, R. B. Schoch, A. L. Stevens, S. R. Tannenbaum, J. Han(2007), *Nat Nanotechnol*, **2**, 121.
23. H. Craighead(2006), *Nature*, **442**, 387.
24. T. Tofteberg, H. Amedro, E. Andreassen(2008), *Polym Eng Sci*, **48**, 2134.
25. C. W. Luo, Y. C. Chiang, H. C. Cheng, C. Z. Wu, C. F. Huang, C. W. Wu, Y. K. Shen, Y. Lin(2011), *Polym Eng Sci*, **51**, 391.
26. J. Giboz, T. Copponnex, P. Mele(2007), *i*, **17**, R96.
27. A. W. McFarland, M. A. Poggi, L. A. Bottomley, J. S. Colton(2005), *Nanotechnology*, **16**, 1249.
28. H. Pranov, H. K. Rasmussen, N. B. Larsen, N. Gadegaard(2005), *Polym Eng Sci*, **46**, 160.
29. U. M. Attia, S. Marson, J. R. Alcock(2009), *Microfluid Nanofluid*, **7**, 1.
30. R. Truckenmuller, S. Giselbrecht, N. Rivron, E. Gottwald, V. Saile, A. van den Berg, M. Wessling, C. van Blitterswijk(2009), *Adv Mater*, **23**, 1311.
31. J. G. Lee, B. K. Lee, T. G. Kang, T. H. Kwon(2010), *Polym Eng Sci*, **50**, 1186.
32. V. Piotter, K. Mueller, K. Plewa, R. Ruprecht, J. Hausselet(2002), *Microsyst Technol*, **8**, 387.